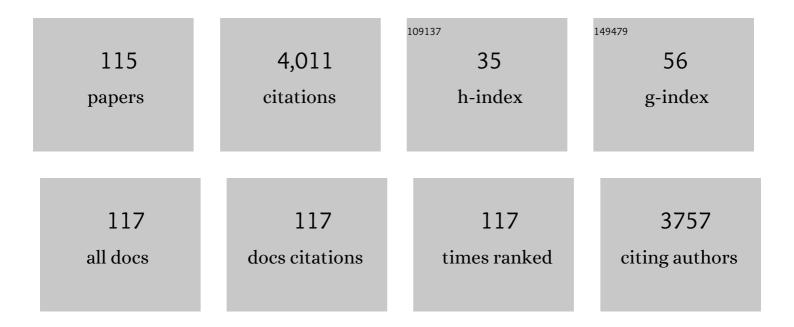
List of Publications by Year in descending order

Source: https://exaly.com/author-pdf/4516993/publications.pdf Version: 2024-02-01



ΙΝΟΗΛΝ ΡΛΝ

#	Article	IF	CITATIONS
1	Layered double hydroxide (LDH) for multi-functionalized corrosion protection of metals: A review. Journal of Materials Science and Technology, 2022, 102, 232-263.	5.6	112
2	Thickness and composition of native oxides and near-surface regions of Ni superalloys. Journal of Alloys and Compounds, 2022, 895, 162657.	2.8	33
3	Hydrogen-Induced Micro-Strain Evolution in Super Duplex Stainless Steel—Correlative High-Energy X-Ray Diffraction, Electron Backscattered Diffraction, and Digital Image Correlation. Frontiers in Materials, 2022, 8, .	1.2	6
4	Reply to Comment on "Corrosion-induced microstructure degradation of copper in sulfide-containing simulated anoxic groundwater studied by synchrotron high-energy X-ray diffraction and ab-initio density functional theory calculation― Corrosion Science, 2022, 199, 110183.	3.0	2
5	Relevance of implicit and explicit solvent in density-functional theory study of adsorption at electrochemical NaCl/Al interface. Materials Today Communications, 2022, 31, 103425.	0.9	1
6	Passivation characteristics of ultra-thin 316L foil in NaCl solutions. Journal of Materials Science and Technology, 2022, 127, 192-205.	5.6	21
7	Temperature effect on mechanical strength and frictional properties of polytetrafluoroethyleneâ€based coreâ€shell nanocomposites. Journal of Applied Polymer Science, 2021, 138, 49929.	1.3	5
8	Corrosion-induced microstructure degradation of copper in sulfide-containing simulated anoxic groundwater studied by synchrotron high-energy X-ray diffraction and ab-initio density functional theory calculation. Corrosion Science, 2021, 184, 109390.	3.0	15
9	Real-Time and Online Lubricating Oil Condition Monitoring Enabled by Triboelectric Nanogenerator. ACS Nano, 2021, 15, 11869-11879.	7.3	56
10	Density Functional Theory Study of Influence of Oxide Thickness and Surface Alloying on Cl Migration within α-Al ₂ O ₃ . Journal of the Electrochemical Society, 2021, 168, 081508.	1.3	10
11	Interactions in Composite Film Formation of Mefp-1/graphene on Carbon Steel. Coatings, 2021, 11, 1161.	1.2	2
12	Towards understanding micro-galvanic activities in localised corrosion of AA2099 aluminium alloy. Electrochimica Acta, 2021, 392, 139005.	2.6	13
13	Comparative study of CNC and CNF as additives in waterborne acrylate-based anti-corrosion coatings. Journal of Dispersion Science and Technology, 2020, 41, 2037-2047.	1.3	11
14	Corrosion inhibition of pre-formed mussel adhesive protein (Mefp-1) film to magnesium alloy. Corrosion Science, 2020, 164, 108309.	3.0	15
15	Anodisation of aluminium alloy AA7075 – Influence of intermetallic particles on anodic oxide growth. Corrosion Science, 2020, 164, 108319.	3.0	31
16	Corrosion- and wear-resistant composite film of graphene and mussel adhesive proteins on carbon steel. Corrosion Science, 2020, 164, 108351.	3.0	22
17	Operando time- and space-resolved high-energy X-ray diffraction measurement to understand hydrogen-microstructure interactions in duplex stainless steel. Corrosion Science, 2020, 175, 108899.	3.0	10
18	Metastable precursor structures in hydrogen-infused super duplex stainless steel microstructure – An operando diffraction experiment. Corrosion Science, 2020, 176, 109021.	3.0	14

#	Article	IF	CITATIONS
19	Studying the Passivity and Breakdown of Duplex Stainless Steels at Micrometer and Nanometer Scales – The Influence of Microstructure. Frontiers in Materials, 2020, 7, .	1.2	12
20	Real-Time Corrosion Monitoring of Aluminum Alloy Using Scanning Kelvin Probe Force Microscopy. Journal of the Electrochemical Society, 2020, 167, 081502.	1.3	23
21	Lateral variation of the native passive film on super duplex stainless steel resolved by synchrotron hard X-ray photoelectron emission microscopy. Corrosion Science, 2020, 174, 108841.	3.0	22
22	Time-resolved grazing-incidence X-ray diffraction measurement to understand the effect of hydrogen on surface strain development in super duplex stainless steel. Scripta Materialia, 2020, 187, 63-67.	2.6	8
23	In-Situ Time-Lapse SKPFM Investigation of Sensitized AA5083 Aluminum Alloy to Understand Localized Corrosion. Journal of the Electrochemical Society, 2020, 167, 141502.	1.3	11
24	Mussel-Inspired Graphene Film with Enhanced Durability as a Macroscale Solid Lubricant. ACS Applied Materials & Interfaces, 2019, 11, 31386-31392.	4.0	22
25	Numerical simulation of micro-galvanic corrosion of Al alloys: Effect of density of Al(OH)3 precipitate. Electrochimica Acta, 2019, 324, 134847.	2.6	17
26	Recent Development of Corrosion Protection Strategy Based on Mussel Adhesive Protein. Frontiers in Materials, 2019, 6, .	1.2	9
27	Characterization of Native Oxide and Passive Film on Austenite/Ferrite Phases of Duplex Stainless Steel Using Synchrotron HAXPEEM. Journal of the Electrochemical Society, 2019, 166, C3336-C3340.	1.3	22
28	Redefining passivity breakdown of super duplex stainless steel by electrochemical operando synchrotron near surface X-ray analyses. Npj Materials Degradation, 2019, 3, .	2.6	36
29	A DFT-Study of Cl Ingress into α-Al ₂ O ₃ (0001) and Al(111) and Its Possible Influence on Localized Corrosion of Al. Journal of the Electrochemical Society, 2019, 166, C3124-C3130.	1.3	25
30	Probing electrochemical mechanism of polyaniline and CeO2 nanoparticles in alkyd coating with in-situ electrochemical-AFM and IRAS. Progress in Organic Coatings, 2019, 132, 399-408.	1.9	11
31	Corrosion protective properties of cellulose nanocrystals reinforced waterborne acrylate-based composite coating. Corrosion Science, 2019, 155, 186-194.	3.0	40
32	Investigation and application of mussel adhesive protein nanocomposite film-forming inhibitor for reinforced concrete engineering. Corrosion Science, 2019, 153, 333-340.	3.0	22
33	Influence of Surface Strain on Passive Film Formation of Duplex Stainless Steel and Its Degradation in Corrosive Environment. Journal of the Electrochemical Society, 2019, 166, C3071-C3080.	1.3	17
34	On the Volta potential measured by SKPFM – fundamental and practical aspects with relevance to corrosion Engineering Science and Technology, 2019, 54, 185-198.	0.7	73
35	Passive film characterisation of duplex stainless steel using scanning Kelvin probe force microscopy in combination with electrochemical measurements. Npj Materials Degradation, 2019, 3, .	2.6	28
36	Insight into the Fabrication of ZnAl Layered Double Hydroxides Intercalated with Organic Anions and Their Corrosion Protection of Steel Reinforced Concrete. Journal of the Electrochemical Society, 2019, 166, C617-C623.	1.3	16

#	Article	IF	CITATIONS
37	Co-Adsorption of H2O, OH, and Cl on Aluminum and Intermetallic Surfaces and Its Effects on the Work Function Studied by DFT Calculations. Molecules, 2019, 24, 4284.	1.7	11
38	Experimental and modelling study of the effect of tempering on the susceptibility to environment-assisted cracking of AISI 420 martensitic stainless steel. Corrosion Science, 2019, 148, 83-93.	3.0	10
39	Corrosion inhibition of aluminium alloy AA6063-T5 by vanadates: Local surface chemical events elucidated by confocal Raman micro-spectroscopy. Corrosion Science, 2019, 148, 237-250.	3.0	43
40	Corrosion Inhibition of Aluminum Alloy AA6063-T5 by Vanadates: Microstructure Characterization and Corrosion Analysis. Journal of the Electrochemical Society, 2018, 165, C116-C126.	1.3	49
41	Volta Potential EvolutionÂof Intermetallics in Aluminum Alloy MicrostructureÂUnder Thin Aqueous Adlayers: A combined DFT and Experimental Study. Topics in Catalysis, 2018, 61, 1169-1182.	1.3	26
42	Combining lithography and capillary techniques for local electrochemical property measurements. Electrochemistry Communications, 2018, 87, 53-57.	2.3	16
43	Micro-galvanic corrosion of Cu/Ru couple in potassium periodate (KIO 4) solution. Corrosion Science, 2018, 137, 184-193.	3.0	25
44	Experimental and Simulation Investigations of Copper Reduction Mechanism with and without Addition of SPS. Journal of the Electrochemical Society, 2018, 165, D604-D611.	1.3	3
45	Hydrogen embrittlement of super duplex stainless steel – Towards understanding the effects of microstructure and strain. International Journal of Hydrogen Energy, 2018, 43, 12543-12555.	3.8	44
46	Nano-scale mechanical and wear properties of a waterborne hydroxyacrylic-melamine anti-corrosion coating. Applied Surface Science, 2018, 457, 548-558.	3.1	29
47	In-situ synchrotron GIXRD study of passive film evolution on duplex stainless steel in corrosive environment. Corrosion Science, 2018, 141, 18-21.	3.0	32
48	Numerical Simulation of Micro-Galvanic Corrosion in Al Alloys: Effect of Geometric Factors. Journal of the Electrochemical Society, 2017, 164, C75-C84.	1.3	48
49	Tunable Adsorption and Film Formation of Mussel Adhesive Protein by Potential Control. Langmuir, 2017, 33, 8749-8756.	1.6	6
50	Heating-Induced Enhancement of Corrosion Protection of Carbon Steel by a Nanocomposite Film Containing Mussel Adhesive Protein. Journal of the Electrochemical Society, 2017, 164, C188-C193.	1.3	6
51	Correlative Microstructure Analysis and In Situ Corrosion Study of AISI 420 Martensitic Stainless Steel for Plastic Molding Applications. Journal of the Electrochemical Society, 2017, 164, C85-C93.	1.3	52
52	Integration of electrochemical and synchrotron-based X-ray techniques for in-situ investigation of aluminum anodization. Electrochimica Acta, 2017, 241, 299-308.	2.6	19
53	Temperature-dependent surface nanomechanical properties of a thermoplastic nanocomposite. Journal of Colloid and Interface Science, 2017, 494, 204-214.	5.0	15
54	In Situ AFM Study of Localized Corrosion Processes of Tempered AISI 420 Martensitic Stainless Steel: Effect of Secondary Hardening. Journal of the Electrochemical Society, 2017, 164, C810-C818.	1.3	22

#	Article	IF	CITATIONS
55	Local surface mechanical properties of PDMS-silica nanocomposite probed with Intermodulation AFM. Composites Science and Technology, 2017, 150, 111-119.	3.8	37
56	First-Principle Calculation of Volta Potential of Intermetallic Particles in Aluminum Alloys and Practical Implications. Journal of the Electrochemical Society, 2017, 164, C465-C473.	1.3	61
57	Numerical Simulation of Micro-Galvanic Corrosion in Al Alloys: Steric Hindrance Effect of Corrosion Product. Journal of the Electrochemical Society, 2017, 164, C1035-C1043.	1.3	21
58	Numerical Simulation of Micro-Galvanic Corrosion of Al Alloys: Effect of Chemical Factors. Journal of the Electrochemical Society, 2017, 164, C768-C778.	1.3	24
59	Controllable degradation of medical magnesium by electrodeposited composite films of mussel adhesive protein (Mefp-1) and chitosan. Journal of Colloid and Interface Science, 2016, 478, 246-255.	5.0	18
60	Corrosion Protection and Self-Healing of a Nanocomposite Film of Mussel Adhesive Protein and CeO ₂ Nanoparticles on Carbon Steel. Journal of the Electrochemical Society, 2016, 163, C545-C552.	1.3	20
61	Towards the mechanism of electrochemical activity and self-healing of 1 wt% PTSA doped polyaniline in alkyd composite polymer coating: combined AFM-based studies. RSC Advances, 2016, 6, 19111-19127.	1.7	18
62	In Situ and Operando AFM and EIS Studies of Anodization of Al 6060: Influence of Intermetallic Particles. Journal of the Electrochemical Society, 2016, 163, C609-C618.	1.3	48
63	Corrosion Investigations of Ruthenium in Potassium Periodate Solutions Relevant for Chemical Mechanical Polishing. Journal of Electronic Materials, 2016, 45, 4067-4075.	1.0	11
64	Atmospheric corrosion of Cu, Zn, and Cu–Zn alloys protected by self-assembled monolayers of alkanethiols. Surface Science, 2016, 648, 170-176.	0.8	28
65	A FEM model for investigation of micro-galvanic corrosion of Al alloys and effects of deposition of corrosion products. Electrochimica Acta, 2016, 192, 310-318.	2.6	76
66	Multifunctional commercially pure titanium for the improvement of bone integration: Multiscale topography, wettability, corrosion resistance and biological functionalization. Materials Science and Engineering C, 2016, 60, 384-393.	3.8	32
67	Localized Corrosion of Binary Mg–Ca Alloy in 0.9Âwt% Sodium Chloride Solution. Acta Metallurgica Sinica (English Letters), 2016, 29, 46-57.	1.5	23
68	Active corrosion protection by conductive composites of polyaniline in a UV-cured polyester acrylate coating. Progress in Organic Coatings, 2016, 90, 154-162.	1.9	43
69	Corrosion protection by hydrophobic silica particle-polydimethylsiloxane composite coatings. Corrosion Science, 2015, 99, 89-97.	3.0	69
70	The thickness of native oxides on aluminum alloys and single crystals. Applied Surface Science, 2015, 349, 826-832.	3.1	174
71	In-situ AFM and EIS study of a solventborne alkyd coating with nanoclay for corrosion protection of carbon steel. Progress in Organic Coatings, 2015, 87, 179-188.	1.9	54
72	Corrosion Inhibition of Two Brass Alloys by Octadecanethiol in Humidified Air with Formic Acid. Corrosion, 2015, 71, 908-917.	0.5	6

#	Article	IF	CITATIONS
73	Long-term corrosion protection by a thin nano-composite coating. Applied Surface Science, 2015, 357, 2333-2342.	3.1	21
74	In Situ AFM and Electrochemical Study of a Waterborne Acrylic Composite Coating with CeO ₂ Nanoparticles for Corrosion Protection of Carbon Steel. Journal of the Electrochemical Society, 2015, 162, C610-C618.	1.3	25
75	In-Situ AFM and EIS Study of Waterborne Acrylic Latex Coatings for Corrosion Protection of Carbon Steel. Journal of the Electrochemical Society, 2015, 162, C55-C63.	1.3	28
76	EIS and in situ AFM study of barrier property and stability of waterborne and solventborne clear coats. Progress in Organic Coatings, 2014, 77, 600-608.	1.9	22
77	Influence of polyaniline and ceria nanoparticle additives on corrosion protection of a UV-cure coating on carbon steel. Corrosion Science, 2014, 84, 189-197.	3.0	84
78	Direct Electrochemical Synthesis of Reduced Graphene Oxide (rGO)/Copper Composite Films and Their Electrical/Electroactive Properties. ACS Applied Materials & Interfaces, 2014, 6, 7444-7455.	4.0	127
79	Direct Measurement of Colloidal Interactions between Polyaniline Surfaces in a UV-Curable Coating Formulation: The Effect of Surface Hydrophilicity/Hydrophobicity and Resin Composition. Langmuir, 2014, 30, 1045-1054.	1.6	15
80	Role of microstructure on corrosion initiation of an experimental tool alloy: A Quantitative Nanomechanical Property Mapping study. Corrosion Science, 2014, 89, 236-241.	3.0	7
81	Nanoscale Electrical and Mechanical Characteristics of Conductive Polyaniline Network in Polymer Composite Films. ACS Applied Materials & Interfaces, 2014, 6, 19168-19175.	4.0	35
82	Octadecanethiol as Corrosion Inhibitor for Zinc and Patterned Zinc-Copper in Humidified Air with Formic Acid. Journal of the Electrochemical Society, 2014, 161, C330-C338.	1.3	16
83	Microstructure and transformation temperatures in rapid solidified Ni–Ti alloys. Part II: The effect of copper addition. Journal of Alloys and Compounds, 2014, 589, 633-642.	2.8	9
84	Tribological Properties Mapping: Local Variation in Friction Coefficient and Adhesion. Tribology Letters, 2013, 50, 387-395.	1.2	14
85	The effect of superhydrophobic wetting state on corrosion protection – The AKD example. Journal of Colloid and Interface Science, 2013, 412, 56-64.	5.0	68
86	Study of corrosion behavior of a 22% Cr duplex stainless steel: Influence of nano-sized chromium nitrides and exposure temperature. Electrochimica Acta, 2013, 113, 280-289.	2.6	50
87	In situ confocal Raman micro-spectroscopy and electrochemical studies of mussel adhesive protein and ceria composite film on carbon steel in salt solutions. Electrochimica Acta, 2013, 107, 276-291.	2.6	31
88	Micro-Galvanic Corrosion Effects on Patterned Copper-Zinc Samples during Exposure in Humidified Air Containing Formic Acid. Journal of the Electrochemical Society, 2013, 160, C423-C431.	1.3	23
89	In situ investigations of Fe3+ induced complexation of adsorbed Mefp-1 protein film on iron substrate. Journal of Colloid and Interface Science, 2013, 404, 62-71.	5.0	28
90	Microstructure influence on corrosion behavior of a Fe–Cr–V–N tool alloy studied by SEM/EDS, scanning Kelvin force microscopy and electrochemical measurement. Corrosion Science, 2013, 66, 153-159.	3.0	22

#	Article	IF	CITATIONS
91	UVâ€curable acrylateâ€based nanocomposites: effect of polyaniline additives on the curing performance. Polymers for Advanced Technologies, 2013, 24, 668-678.	1.6	21
92	Radial Spreading of Localized Corrosion-Induced Selective Leaching on α-Brass in Dilute NaCl Solution. Corrosion, 2013, 69, 468-476.	0.5	7
93	Influence of Grain Boundaries on Dissolution Behavior of a Biomedical CoCrMo Alloy: In-Situ Electrochemical-Optical, AFM and SEM/TEM Studies. Journal of the Electrochemical Society, 2012, 159, C422-C427.	1.3	39
94	Electrochemical, atomic force microscopy and infrared reflection absorption spectroscopy studies of pre-formed mussel adhesive protein films on carbon steel for corrosion protection. Thin Solid Films, 2012, 520, 7136-7143.	0.8	18
95	Probing the vertical profiles of potential in a thin layer of solution closed to electrode surface during localized corrosion of stainless steel. Corrosion Science, 2012, 61, 242-245.	3.0	17
96	Engineering of bone fixation metal implants biointerface—Application of parylene C as versatile protective coating. Materials Science and Engineering C, 2012, 32, 2431-2435.	3.8	28
97	Thin Composite Films of Mussel Adhesive Proteins and Ceria Nanoparticles on Carbon Steel for Corrosion Protection. Journal of the Electrochemical Society, 2012, 159, C364-C371.	1.3	23
98	Silane–parylene coating for improving corrosion resistance of stainless steel 316L implant material. Corrosion Science, 2011, 53, 296-301.	3.0	111
99	Toward Homogeneous Nanostructured Polyaniline/Resin Blends. ACS Applied Materials & Interfaces, 2011, 3, 1681-1691.	4.0	45
100	Study of PANI-MeSA conducting polymer dispersed in UV-curing polyester acrylate on galvanized steel as corrosion protection coating. Progress in Organic Coatings, 2011, 70, 108-115.	1.9	41
101	Electrochemical impedance spectroscopy of pure copper exposed in bentonite under oxic conditions. Electrochimica Acta, 2011, 56, 7862-7870.	2.6	34
102	Influence of metal carbides on dissolution behavior of biomedical CoCrMo alloy: SEM, TEM and AFM studies. Electrochimica Acta, 2011, 56, 9413-9419.	2.6	112
103	Scanning Kelvin probe force microscopy study of chromium nitrides in 2507 super duplex stainless steel—Implications and limitations. Electrochimica Acta, 2011, 56, 1792-1798.	2.6	75
104	Electrochemical and AFM studies of mussel adhesive protein (Mefp-1) as corrosion inhibitor for carbon steel. Electrochimica Acta, 2011, 56, 1636-1645.	2.6	87
105	Minuscule device for hydrogen generation/electrical energy collection system on aluminum alloy surface. International Journal of Hydrogen Energy, 2011, 36, 2855-2859.	3.8	7
106	Study of nobility of chromium nitrides in isothermally aged duplex stainless steels by using SKPFM and SEM/EDS. Corrosion Science, 2010, 52, 179-186.	3.0	120
107	Investigation of Influence of Small Particles in MP35N on the Corrosion Resistance in Synthetic Biological Environment. Journal of the Electrochemical Society, 2009, 156, C341.	1.3	3
108	Depletion effects at phase boundaries in 2205 duplex stainless steel characterized with SKPFM and TEM/EDS. Corrosion Science, 2009, 51, 1850-1860.	3.0	170

#	Article	IF	CITATIONS
109	Localized corrosion behaviour of reinforcement steel in simulated concrete pore solution. Corrosion Science, 2009, 51, 2130-2138.	3.0	102
110	An electrochemical impedance spectroscopy study of copper in a bentonite/saline groundwater environment. Electrochimica Acta, 2008, 53, 7556-7564.	2.6	31
111	Electrochemical behavior and anticorrosion properties of modified polyaniline dispersed in polyvinylacetate coating on carbon steel. Electrochimica Acta, 2008, 53, 4239-4247.	2.6	75
112	Characterization of Phases in Duplex Stainless Steel by Magnetic Force Microscopy/Scanning Kelvin Probe Force Microscopy. Electrochemical and Solid-State Letters, 2008, 11, C41.	2.2	51
113	Nickel release from nickel particles in artificial sweat. Contact Dermatitis, 2007, 56, 325-330.	0.8	24
114	Tafel slopes used in monitoring of copper corrosion in a bentonite/groundwater environment. Corrosion Science, 2005, 47, 3267-3279.	3.0	42
115	Determination of instantaneous corrosion rates and runoff rates of copper from naturally patinated copper during continuous rain events. Corrosion Science, 2002, 44, 2131-2151.	3.0	86